Anal. Chem. **2007,** *79,* 3673−3689

Metal-Assisted Secondary Ion Mass Spectrometry Using Atomic (Ga^+, In^+) and Fullerene Projectiles

A. Delcorte,*,† S. Yunus,† N. Wehbe,† N. Nieuwjaer,†,# C. Poleunis,† A. Felten,‡ L. Houssiau,‡ J.-J. Pireaux,‡ and P. Bertrand†

PCPM, Université Catholique de Louvain, Croix du Sud 1, B-1348 Louvain-la-Neuve, Belgium, and LISE, Facultés Universitaires Notre-Dame de la Paix, Namur, Belgium

The advantages and drawbacks of using either monatomic or buckminsterfullerene primary ions for metal-assisted secondary ion mass spectrometry (MetA-SIMS) are investigated using a series of organic samples including additive molecules, polyolefins, and small peptides. Gold deposition is mostly performed by sputter-coating, and in some cases, the results are compared to those of thermal evaporation (already used in a previous article: Delcorte, A.; Médard, N.; Bertrand, P. *Anal. Chem.* 2002, *74*, 4955). The microstructure of the gold-covered sample surfaces is assessed by scanning and transmission electron microscopies. The merits of the different sets of experimental conditions are established via the analysis of fragment and parent-like ion yields. For most of the analyzed samples, the highest yields of fragment and parent-like ions are already reached with the sole use of C_{60}^+ projectiles. Metallization of the sample does not lead to a significant additional enhancement. For polyethylene and polypropylene, however, gold metallization associated with Ga^+/In^+ projectiles appears to be the only way to observe large cationized, sample-specific chain segments ($m/z \sim 1000-2000$). A detailed study of the polypropylene mass spectra as a function of gold coverage shows that the dynamics of yield enhancement by metal nanoparticles is strongly dependent on the choice of the projectile, e.g., a pronounced increase with Ga^+ and a slow decay with C_{60}^+. The cases of Irganox 1010, a polymer antioxidant, and leucine enkephalin, a small peptide, allow us to investigate the specific influence of the experimental conditions on the emission of parent-(like) ions such as M^+, $(M + Na)^+$, and $(M + Au)^+$. The results show a dependence on both the type of sample and the considered secondary ion. Using theoretical and experimental arguments, the discussion identifies some of the mechanisms underlying the general trends observed in the results. Guidelines concerning the choice of the experimental conditions for MetA-SIMS are provided.

The quest for higher sensitivity is at the top of the preoccupations for scientists working in the field of organic secondary ion mass spectrometry (SIMS).[1] Even with polyatomic ion sources such as Au_3^+, Bi_n^+, and C_{60}^+, the relative ionization yields of organic molecules and fragments, valuable for chemical identification and localization on the surface, remain very low. While recent molecular dynamics simulations and experimental studies show that a single fullerene projectile can desorb about 10^2 molecules,[2,3] the actually measured ion yield is rather of the order of 10^{-4} to 10^{-2}. This large gap shows the extent of the signal that might be gained if molecular ionization could be enhanced.

In addition to the use of more efficient projectile sources,[4−6] another route for molecular ion yield enhancement consists in devising new sample preparation procedures. Such preparation methods aimed at improving sensitivity in SIMS have been grouped under the term matrix-enhanced SIMS or ME-SIMS. They usually rely on the chemical matrix effect provided by the addition of molecules,[7,8] salts,[9,10] or even metal nanoparticles[11,12] to the sample, which induces ionization enhancement via various mechanisms including proton transfer, cationization by metal ions, and possibly, lowering of the molecular ionization potential. Because the observed effects and the physics at play appear related, the use of specific substrates such as noble metals[13,14] can also be associated to a broad definition of ME-SIMS. The literature concerning matrix and substrate enhancement actually encompasses a time span of about 30 years. The latest developments in the field (including high-resolution imaging), following the breakthrough of matrix-assisted laser desorption ionization (MALDI) as a powerful technique for biological molecule characterization, have been discussed recently.[15,16]

* To whom correspondence should be addressed. Fax: 32-10-473-452. E-mail: delcorte@pcpm. ucl.ac.be.

† PCPM, Université Catholique de Louvain.

‡ LISE, Facultés Universitaires Notre-Dame de la Paix.

Current address: LPMCN, Université Claude Bernard Lyon I and CNRS, 43 Bd du 11 Novembre 1918, 69622 Villeurbanne Cedex, France.

(1) Vickerman, J. C. In *ToF-SIMS: Surface Analysis by Mass Spectrometry*; Vickerman, J. C., Briggs, D., Eds.; SurfaceSpectra/IMPublications: Chichester, U.K., 2001; Chapter 1.
(2) Winograd, N.; Postawa, Z.; Cheng, J.; Szakal, C.; Kozole, J.; Garrison, B. J. *App. Surf. Sci.* **2006**, *252*, 6836.
(3) Delcorte, A.; Garrison, B. J. *Nucl. Instrum. Methods Phys. Res., Sect. B* **2007**, *255*, 223.
(4) Gillen, G.; Fahey, A. *Appl. Surf. Sci.* **2003**, *203*, 209.
(5) Weibel, D.; Wong, S.; Lockyer, N.; Blenkinsopp, P.; Hill, R.; Vickerman, J. C. *Anal. Chem.* **2003**, *75*, 1754.
(6) Kollmer, F. *Appl. Surf. Sci.* **2004**, *231−232*, 153.
(7) Wu, K. J.; Odom, R. W. *Anal. Chem.* **1996**, *68*, 873.
(8) Wittmaak, K.; Szymczak, W.; Hoheisel, G.; Tuszynski, W. *J. Am. Soc. Mass Spectrom.* **2000**, *11*, 553.
(9) Grade, H.; Cooks, R. G. *J. Am. Chem. Soc.* **1978**, *100*, 5615.
(10) Delcorte, A.; Bertrand, P. *Anal. Chem.* **2005**, *77*, 2107.
(11) Delcorte, A.; Médard, N.; Bertrand, P. *Anal. Chem.* **2002**, *74*, 4955.
(12) Marcus, A.; Winograd, N. *Anal. Chem.* **2006**, *78*, 141.
(13) Grade, H.; Winograd, N.; Cooks, R. G. *J. Am. Chem. Soc.* **1977**, *99*, 7725.
(14) Bletsos, I. V.; Hercules, D. M.; van Leyen, D.; Hagenhoff, B.; Niehuis, E.; Benninghoven, A. *Anal. Chem.* **1991**, *63*, 1953.

10.1021/ac062406l CCC: $37.00
Published on Web 04/07/2007

Among these methods, the condensation of noble metal nanoparticles on the surface to be analyzed appears very attractive for several reasons: (i) the yield enhancement reaches about 1 order of magnitude for characteristic fragments and often more for parent molecules; (ii) the method is simpler and maybe more universal ("one metal fits all") than the MALDI procedure, which requires a certain adequacy between the analyte and the matrix molecules; (iii) it can be readily applied to real world samples; (iv) it is a physical deposition method and, as such, does not involve wet processes that might more easily scramble the specific information present at the surface (dissolution, segregation). The usefulness of the gold metallization procedure has been largely demonstrated in the case of monatomic projectile bombardment (Ga^+,[11,17] In^+,[18,19] Au^+).[20] The main drawback that has been mentioned,[16,21] and should be a concern in any analysis, is the possibility that the metal condensation process might affect the integrity of the surface molecules. Among the most recent reports, it seems fit to mention the detailed SIMS imaging study of cells and tissues by Altelaar et al.[18] Forays into the domains of polyatomic (SF_5^+,[17] C_{60}^+,[22] Bi_n^+)[23] ion bombardment and laser irradiation also exist.[24,25] However, to our knowledge, there has not been a detailed report yet concerning the application of sources of cluster (such as C_{60}^+) in combination with the metallization procedure.

The goal of this study is to assess the possible advantages and drawbacks of using fullerene versus monatomic projectiles for metal-assisted secondary ion mass spectrometry (MetA-SIMS). Several types of samples including bulk polyolefins, polymer additives, and peptides are investigated. The discussion focuses on the interpretation of the general trends observed in results on the basis of recent theoretical and experimental studies of desorption and ionization under irradiation.

MATERIALS AND METHODS

Samples. High-molecular-weight, bulk polyolefin samples, polyethylene (PE) and polypropylene (PP), were cut, respectively, from a bottle cap (Vel) and from a biaxially stretched film (Shell Research). Samples from a polymer additive, Irganox 1010 (IRGA; MW = 1176.8 Da; Ciba Specialty Chemical Inc.), and from an acetate salt of leucine enkephalin (LE; MW = 555.6 Da; Sigma-Aldrich), a small peptide, were dissolved to a concentration of 1 mg/mL. They were then cast on cleaned (2-propanol; hexane) silicon substrates (~1 cm^2) by depositing a droplet of the solution and allowing the solvent to evaporate. Microstructured polymeric samples were obtained using the method of breath figure imprinting,[26] by activation of 2,2,6,6-tetramethyl-1-piperidinyloxyl (TEMPO)-terminated polystyrene (PS) with *p*-toluenesulfonic acid (PTSA).[27] A subset of each of these samples was metallized using a Cressington 208 HR sputter-coater, with a Au fluence of 20 nmol/cm^2. A series of PP samples was metallized by steps of 5 Å (layer-equivalent thickness) up to 40 Å in order to check the dynamics of the yield evolution with increasing gold coverage. Some of the pristine organic samples (IRGA, PP) were also covered with gold via thermal evaporation. Those evaporations were carried out in an Edwards evaporator at an operating pressure of 10^{-6} mbar and a deposition rate of 0.1 nm/s.[11] Samples of plasma polystyrene (PPS) were polymerized from a low-pressure plasma and metallized afterward by evaporating gold under high vacuum with a total fluence of 20 nmol/cm^2 onto their top surface. For all the metallization procedures (sputter-coating and thermal evaporation), the deposited metal amount was measured using a quartz crystal monitor, and the reported values correspond to the assumption that the sticking coefficient is the same on the monitor and the organic samples (see ref 28). For comparison purpose, samples of a PS standard (M_n = 550 Da) were cast on a silver foil from a dilute (0.1 mg/mL) and a more concentrated solution (10 mg/mL). A dilute solution (0.1 mg/mL) made of a mix of several standards (M_n = 2180, 4760, 8000, and 12 400 Da; 1:1:1:1) was also cast on a gold-metallized silicon wafer.

Analytical Techniques. The secondary ion mass analyses were performed in a PHI EVANS time-of-flight (TOF) SIMS (TRIFT 1).[29] To improve the measured intensities, the secondary ions were postaccelerated by a high voltage (7 kV) in front of the detector. No charge compensation was needed. The 15 keV $^{69}Ga^+$ beam was obtained from a FEI 83-2 liquid metal ion source (1.2 nA dc current; 5 kHz frequency; 22 ns pulse width bunched down to 1 ns). The 15 keV C_{60}^+ measurements were conducted using a primary ion (PI) beam system (IOG-C60-20) from Ionoptika Ltd. (2−100 pA dc current with apertures of 300−1000 μm and a 50 V grid voltage).[5] The contribution from C_{60}^{2+} was eliminated by a double set of blanking plates. The PI current was measured in a small aperture of the sample holder, with and without a positive bias of 27 V (to cancel the effects of secondary electron emission). For TOF-SIMS images (and some of the spectral analyses), the samples were bombarded with a pulsed $^{115}In^+$ ion beam (FEI 92-2, 25 keV, 630 pA dc; 11−17 kHz frequency; 28.9 ns pulse width). All the images were recorded with a PI fluence in the range of $2-3.5 \times 10^{13}$ ions/cm^2, which is close to static conditions. In this paper, the secondary ion yield is defined as the measured number of secondary ions per PI, without any correction for the instrument transmission and detection efficiencies.

The scanning electron microscopy (SEM) images were recorded using a Zeiss Leo 982 apparatus (5 keV primary electron beam energy). A Philips Tecnai 10 microscope operating at 100 kV was used for the transmission electron microscopy (TEM) observations.

(15) Delcorte, A. *Appl. Surf. Sci.* **2006**, *252*, 6582.
(16) McDonnell, L. A.; Piersma, S. R.; Altelaar, A. F. M.; Mize, T. H.; Luxembourg, S. L.; Verhaert, P. D. E. M.; van Minnen, J.; Heeren, R. M. A. *J. Mass Spectrom.* **2005**, *40*, 160−168.
(17) Adriaensen, L.; Vangaever, F.; Gijbels, R. *Anal. Chem.* **2004**, *76*, 6777.
(18) Altelaar, A. F. M.; Klinkert, I.; Jalink, K.; de Lange, R. P. J.; Adan, R. A. H.; Heeren, R. M. A.; Piersma, S. R. *Anal. Chem.* **2006**, *78*, 734.
(19) Keune, K.; Boon, J. J. *Surf. Interface Anal.* **2004**, *36*, 1620.
(20) Nygren, H.; Johansson, B. R.; Malmberg, P. *Microsc. Res. Tech.* **2004**, *65*, 282.
(21) Inoue, M.; Murase, A.; Sugiura, M. *Anal. Sci.* **2004**, *20*, 1623.
(22) Delcorte, A.; Poleunis, C.; Bertrand, P. *Appl. Surf. Sci.* **2006**, *252*, 6494.
(23) McDonnell, L. A.; Heeren, R. M. A.; de Lange, R. P. J.; Fletcher, I. *J. Am. Soc. Mass Spectrom.* **2006**, *17*, 1195.
(24) Delcorte, A.; Bour, J.; Aubriet, F.; Muller, J. F.; Bertrand, P. *Anal. Chem.* **2003**, *75*, 6875.
(25) McLean, J. A.; Stumpo, K. A.; Russell, D. H. *J. Am. Chem. Soc.* **2005**, *127*, 5304.
(26) Yunus, S.; Spano, F.; Patrinoiu, G.; Bolognesi, A.; Botta, C.; Brühwiler, D.; Zabala Ruiz, A.; Calzaferri, G. *Adv. Funct. Mater.* **2006**, *16*, 2213.
(27) Yunus, S.; Delcorte, A.; Poleunis, C.; Bertrand, P.; Bolognesi, A.; Botta, C. *Adv. Funct. Mater.*, in press.
(28) Novak, S.; Mauron, R.; Dietler, G.; Schlapbach, L. In *Metallized Plastics 2: Fundamental and Applied Aspects*; Mittal, K. L., Ed.; Plenum Press: New York, 1991; p 233.
(29) Schueler, B. W. *Microsc. Microanal. Microstruct.* **1992**, *3*, 119.

Molecular Dynamics Simulations. The simulation results presented in the Mechanisms of Ion Emission section have been introduced in detail elsewhere. In the model, Hamilton's equations of motion were numerically integrated over a defined time interval (10−50 ps).[30] Forces among the particles in the system were derived from semiempirical interaction potentials. Two approaches were considered: in the coarse-grain modeling of icosane, $C_{20}H_{42}$ (Figure 11a),[3] certain atoms were grouped to form united atoms (CH_2 and CH_3), while in the model of PS tetramers (Figure 11b−e), the sample was described at the atomistic level. The atomistic simulations of PS samples were performed with a system containing 36 192 atoms, forming 464 molecules.[31] The C−C, C−H, and H−H interactions were described by the AIREBO potential. The computational cell for coarse-grained simulations (Figure 11a) of icosane samples was a box containing 256 000 united atoms (793 600 atom equivalents), forming 12 800 molecules. A Morse potential between adjacent CH_2 and CH_3 particles was chosen to account for the dissociating bond stretch term. Lennard-Jones potentials were used for the intermolecular interactions. For the simulations involving silver, the Ag−Ag interactions were described by the MD−MC corrected effective medium (CEM) potential, and the Ag−C and Ag−H interactions were described by Lennard-Jones potential functions. In all the simulations, the AIREBO potential was used to describe the C−C interaction of the C_{60} projectile.

RESULTS AND DISCUSSION

In the first step of the physical vapor deposition process, nonreactive metals such as gold and silver tend to form clusters on the surface of organic samples, because of the unbalance between the metal−metal and the metal−organic forces.[32,33] Figure 1 shows the scanning electron micrographs of two samples sputter-coated with 20 Å of gold (20 nmol/cm^2), as indicated by a quartz crystal microbalance. The top frame corresponds to a silicon surface and the bottom frame to a dried droplet of LE cast on silicon from a mixed ethanol/water solution (50/50 vol %). In both cases, a pattern of coalescing gold islets is clearly visible against the sample background. As discussed in a previous article,[11] this dose corresponds to a maximum yield enhancement for Au-cationized molecular ions in SIMS of PS standard samples (Ga^+ ion bombardment). In the following subsections, the molecular ion yields measured for several types of samples with the combined use of Ga^+ and gold islets will be compared to those observed using C_{60}^+ projectiles instead of gallium.

Polyolefin Films. 1. Polyethylene and Polypropylene. Polyethylene and polypropylene are archetypal polymeric materials, as widely used in everyday life as they are thoroughly studied in the laboratory. For this study, two commercial samples were used, a PE bottle cap and a biaxially stretched PP film. The mass spectra of these polymers under gallium bombardment have been largely discussed in the literature.[34,35] Even though the chemical structures of these two polymers are very similar, they can be distinguished by comparing the intensities of the $C_xH_y^+$ secondary ions present in the fingerprint region of their mass spectra, in the range of 0−150 amu. In particular, the deprotonated monomer ($C_3H_5^+$; $m/z = 41$) usually dominates the positive mass spectrum of PP and the relative intensity of the peak $C_5H_9^+$ ($m/z = 69$) is comparatively larger.

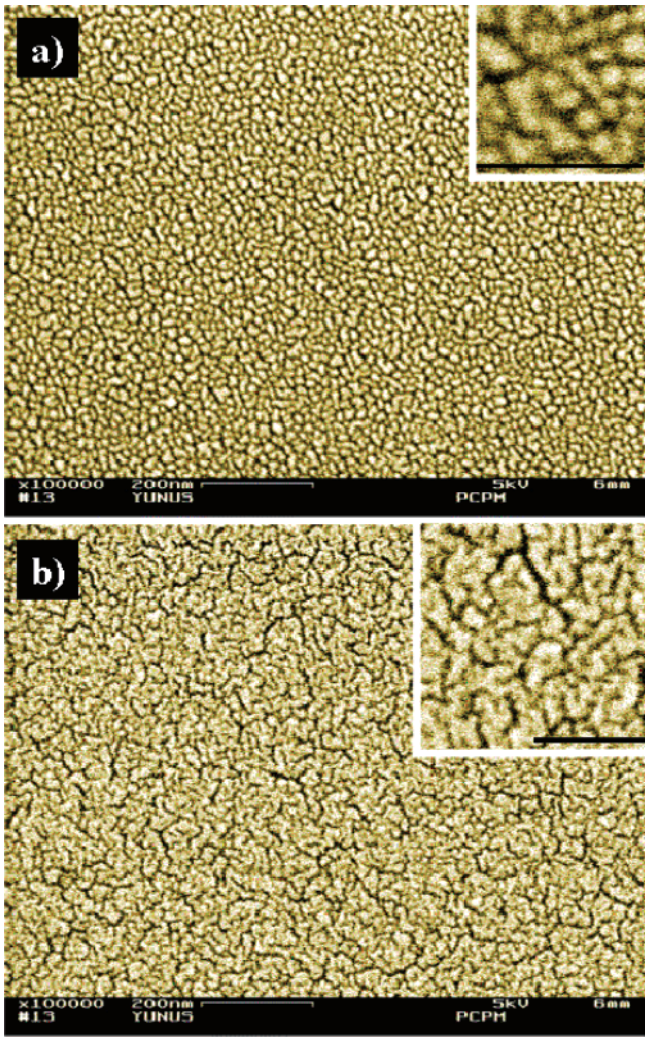

Figure 1. Scanning electron microscope (SEM) images of (a) a Au-metallized silicon wafer; (b) a Au-metallized dried droplet of leucine enkephalin salt on silicon (20 nmol/cm^2 Au, sputter-coated). The bar in the insets is 100 nm long.

Figure 2, parts a and b, shows the measured ion yields of several of the most intense fingerprint peaks of PP and PE, respectively. The different groups of bars correspond to different projectiles and samples, as explained in the figure caption. This figure format will be used in several instances along the article. First, the results obtained with Ga^+ projectiles confirm a previous report where similar samples were investigated. The deposition of gold on the surface results in an average yield enhancement that is close to 1 order of magnitude (see indicative values on the bar graphs). The central columns in Figure 2a also show the yields obtained for the bombardment of a Au-metallized sample of PP by In^+ ions. In comparison with Ga^+, the use of In^+ results in an additional increase of the characteristic ion yields by a factor of

(30) Garrison, B. J. In *ToF-SIMS: Surface Analysis by Mass Spectrometry*; Vickerman, J. C., Briggs, D., Eds.; SurfaceSpectra/IMPublications: Chichester, U.K., 2001; p 223.
(31) Delcorte, A.; Garrison, B. J. *J. Phys. Chem. B* **2004**, *108*, 15652.
(32) Travaly, Y.; Bertrand, P. *Surf. Interface Anal.* **1995**, *23*, 328.
(33) Travaly, Y.; Zhang, L.; Zhao, Y.; Pfeffer, R.; Uhrich, K.; Cosandey, F.; Garfunkel, E.; Madey, T. E. *J. Mater. Res.* **1999**, *14*, 3673.
(34) Lianos, L.; Quet, C.; Tran, M. D. *Surf. Interface Anal.* **1994**, *21*, 14.
(35) Delcorte, A.; Weng, L.-T.; Bertrand, P. *Nucl. Instrum. Methods Phys. Res., Sect. B* **1995**, *100*, 213.

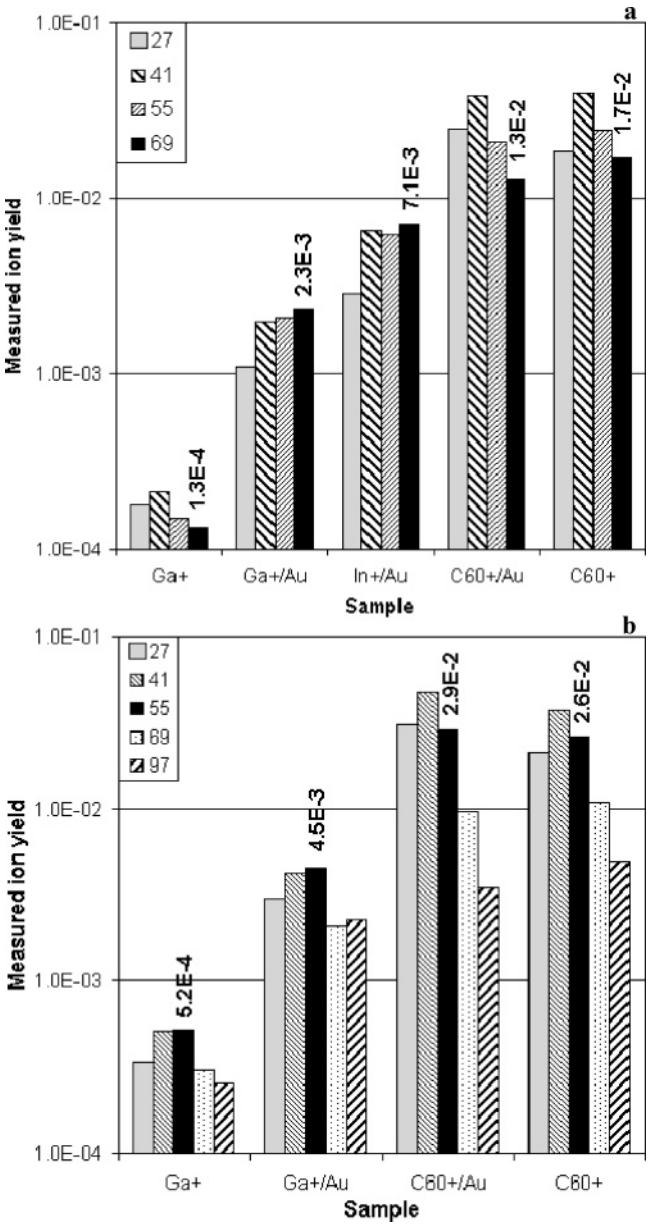

Figure 2. Measured yields of (a) PP and (b) PE fingerprint secondary ions obtained with different experimental conditions, including three types of projectiles (Ga^+, In^+, C_{60}^+) and two sample preparations (pristine and sputter-coated with 20 nmol/cm^2 Au). The secondary ions are signified by their mass/charge ratio in the bar graphs ($C_2H_3^+$, $m/z = 27$; $C_3H_5^+$, $m/z = 41$; $C_4H_7^+$, $m/z = 55$; $C_5H_9^+$, $m/z = 69$; $C_7H_{13}^+$, $m/z = 97$).

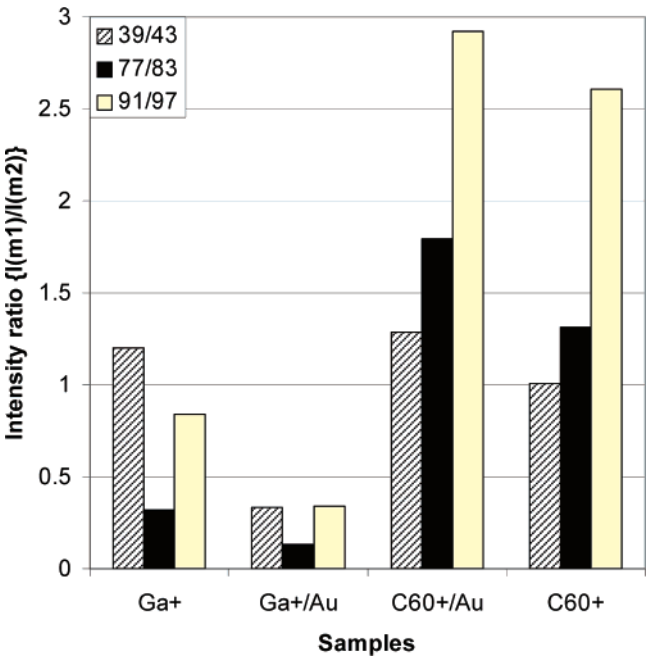

Figure 3. Dependence of the secondary ion intensity ratios [$I\{39\ m/z\}/I\{43\ m/z\}$, $I\{77\ m/z\}/I\{83\ m/z\}$, $I\{91\ m/z\}/I\{97\ m/z\}$] used as indicators of unsaturation and cyclic structures in the secondary ion flux, as a function of the experimental conditions (considered ions: $C_3H_3^+$, $m/z = 39$; $C_3H_7^+$, $m/z = 43$; $C_6H_5^+$, $m/z = 77$; $C_6H_{11}^+$, $m/z = 83$; $C_7H_7^+$, $m/z = 91$; $C_7H_{13}^+$, $m/z = 97$).

~3. For both monatomic projectile cases, the application of a gold coverage also changes the relative intensities of the fingerprint ions of PP. In particular, the yield enhancement of $C_4H_7^+$ ($m/z = 55$) and $C_5H_9^+$ ($m/z = 69$) are more pronounced than those of smaller fragments such as $C_2H_3^+$ ($m/z = 27$) and $C_3H_5^+$ ($m/z = 41$).

As was reported for other bulk polymers,[5] the absolute yields are about 2 orders of magnitude larger using C_{60}^+ instead of Ga^+ (Figure 2). In sharp contrast with the case of gallium projectiles, the condensation of a gold layer on the surface *does not* induce a yield increase for C_{60}^+ bombardment. Overall, the small yield difference observed between pristine and metallized samples upon fullerene bombardment is insignificant, given the uncertainty affecting the measurement of the (low) C_{60}^+ ion current and its variation from day to day (for PP, a full set of measurements obtained in a small time interval will be discussed with more confidence hereafter). Nonetheless, the results (Figure 2) show quite generally that, under fullerene bombardment, the metallization procedure induces a small relative intensity drop for high-mass characteristic ions ($C_5H_9^+$; $m/z = 69$) and a slight increase for low-mass ions ($C_2H_3^+$; $m/z = 27$).

Another effect concerns the relative fractions of unsaturated and saturated secondary ions. Several intensity ratios providing information about the degree of unsaturation of the observed hydrocarbon ions are reported in Figure 3 as a function of the experimental conditions. First of all, the proportions of cyclic fragments such as $C_6H_5^+$ ($m/z = 77$) and $C_7H_7^+$ ($m/z = 91$) are much larger using fullerene instead of gallium projectiles, as shown by the ratios $I\{77\ m/z\}/I\{83\ m/z\}$ and $I\{91\ m/z\}/I\{97\ m/z\}$. The formation of these cyclic structures under "static" bombardment conditions is indicative of the damage directly created by the projectile in the energized nanovolume surrounding the impact point. The variation of the ratio $I\{39\ m/z\}/I\{43\ m/z\}$, corresponding to smaller ions, is much less pronounced. Upon gold metallization of the samples, the evolution of all these ratios strongly depends on the type of projectile used. For gallium bombardment, all the indicators of unsaturation decrease after metallization, i.e., the enhancement of saturated ion yields, directly mirroring the structure of the polymer, is larger than that of unsaturated ions, which are characteristic of damage. In the case of fullerene bombardment, these indicators all tend to increase slightly. Between the Ga^+- and the C_{60}^+-bombarded Au/metallized PP samples, the ratios $I\{77\ m/z\}/I\{83\ m/z\}$ and $I\{91\ m/z\}/I\{97\ m/z\}$ increase by an order of magnitude. Such strong—and opposite—variations clearly reflect differences in the manner by

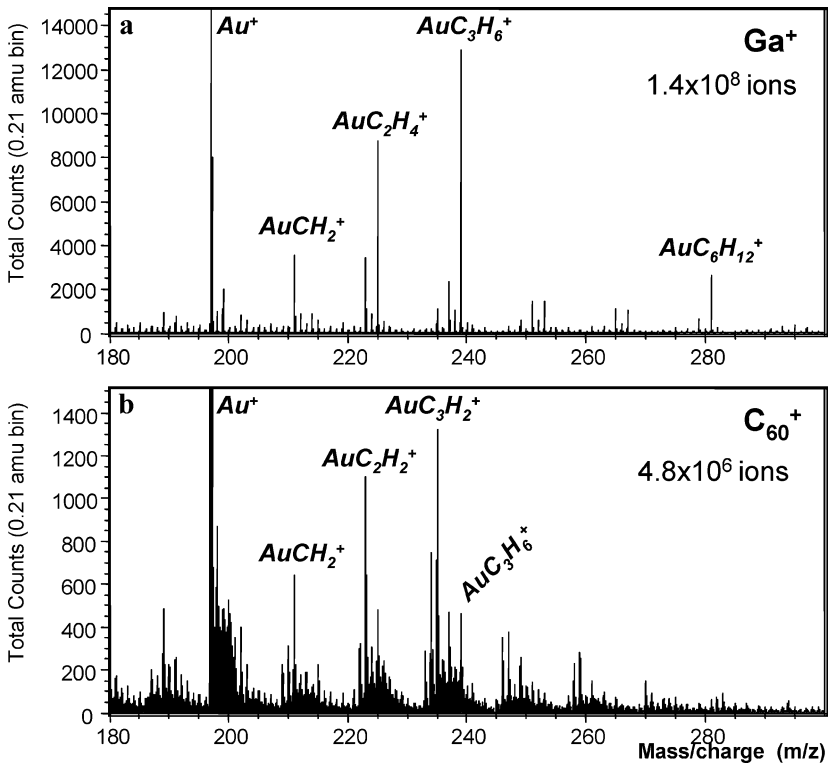

Figure 4. Partial positive secondary ion mass spectra (180 < *m*/*z* < 300) of Au-metallized PP samples upon (a) 15 keV Ga^+ and (b) 15 keV C_{60}^+ bombardment.

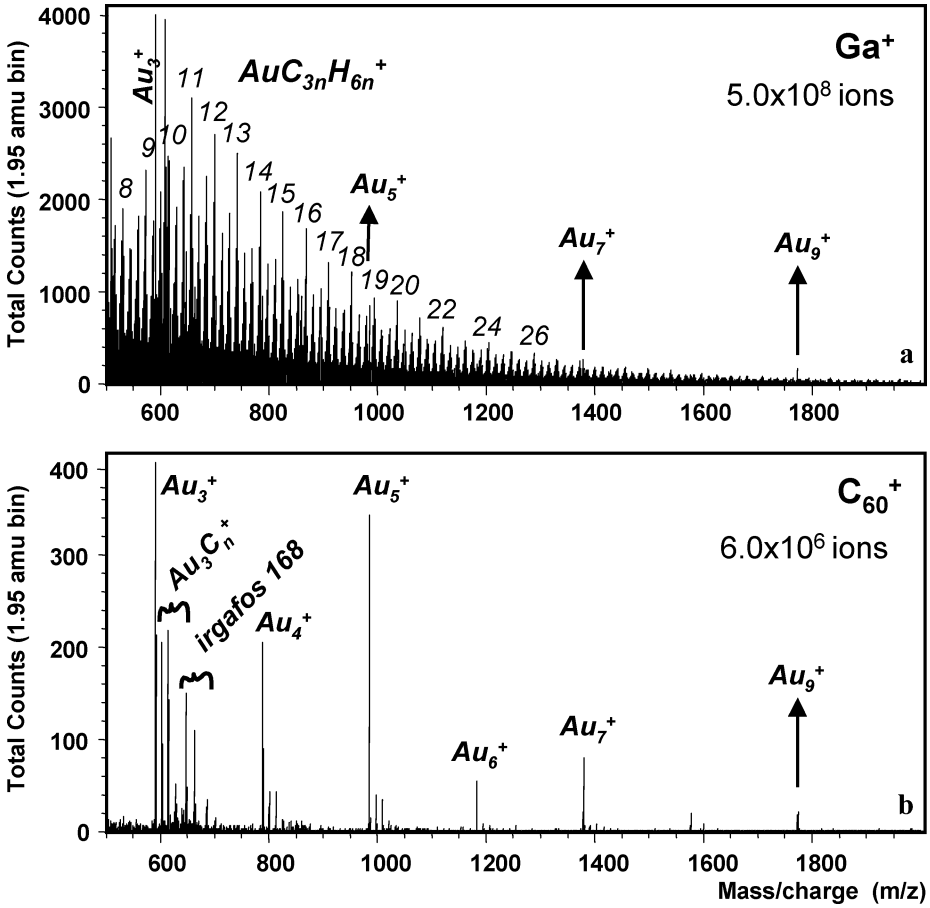

Figure 5. Partial positive secondary ion mass spectra (500 < *m*/*z* < 2000) of Au-metallized PP samples upon (a) 15 keV Ga^+ and (b) 15 keV C_{60}^+ bombardment.

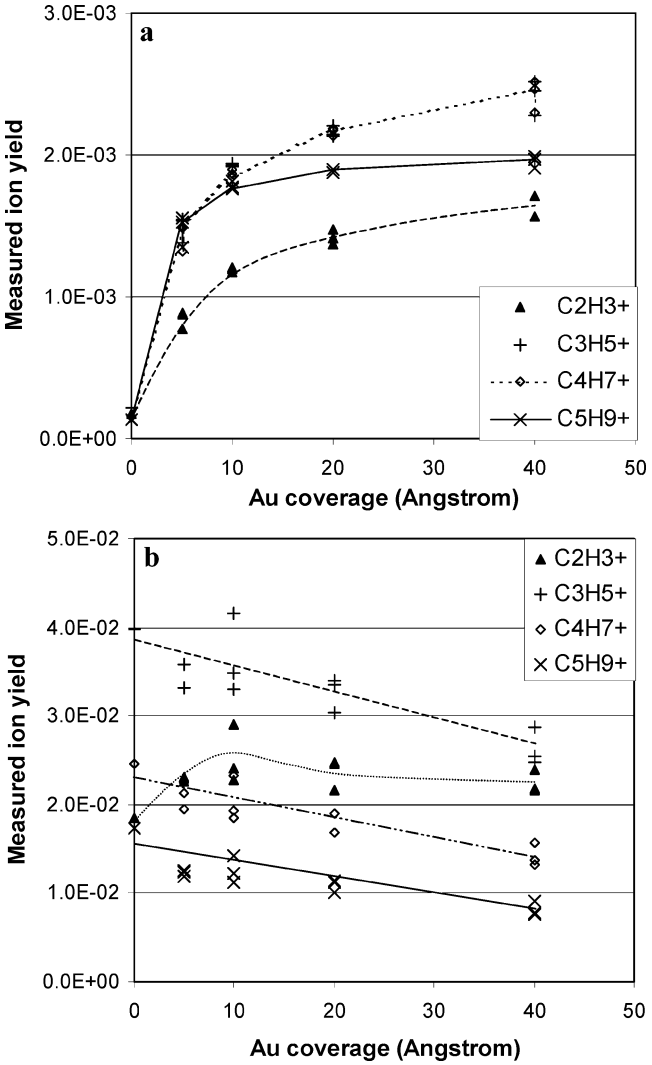

Figure 6. Evolution of the yields of PP positive secondary ions as a function of the gold coverage (full-layer-equivalent thickness in angstroms): (a) 15 keV Ga^+ projectiles; (b) 15 keV C_{60}^+ projectiles.

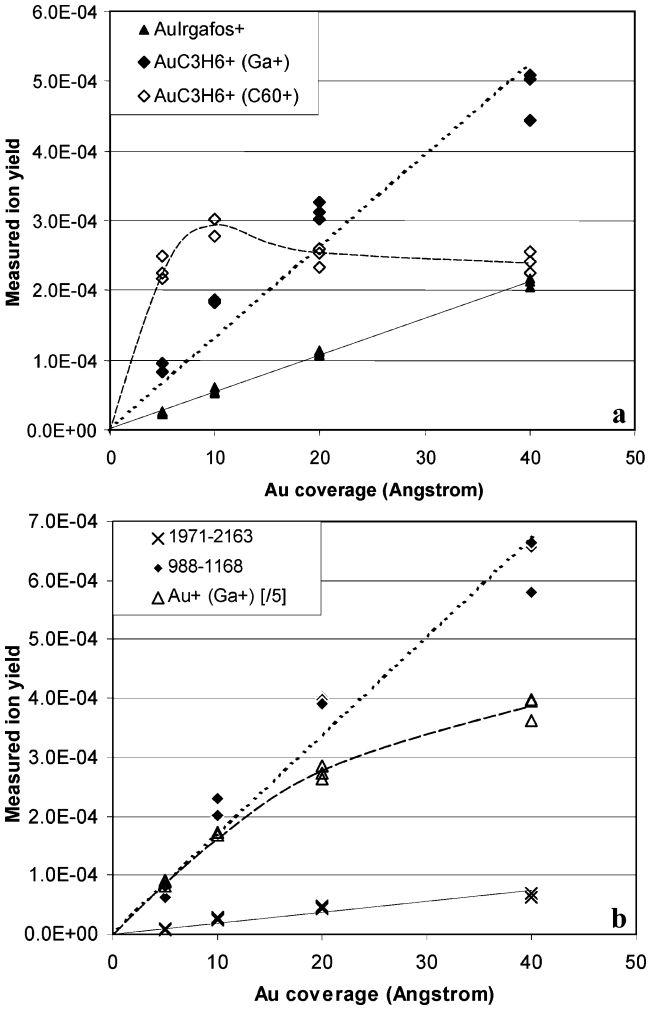

Figure 7. Evolution of the yields of selected ions sputtered from PP as a function of the gold coverage (full-layer-equivalent thickness in angstroms): (a) Au-cationized PP (C_{60}^+ and Ga^+ bombardment) and Irgafos 168 ions (Ga^+ bombardment); (b) Au-cationized chain segments ($988 < m/z < 1168$ and $1971 < m/z < 2163$) and elemental gold ions (Ga^+ bombardment).

which the projectiles impart their energy to the sample surfaces. These differences will be tentatively interpreted in the Mechanisms of Ion Emission section.

In addition to the usual fingerprint fragments of polyolefins, the metallization procedure also gives access to a series of additional adduct ion peaks resulting from the cationization of neutral fragments by the metal. Upon gallium bombardment, it was shown that the cationized monomers of PE, PP, and PS could be detected with a particularly high intensity after gold metallization.[11] These adduct ions provide a complementary means to distinguish between polymers that are very close from a chemical viewpoint (PE and PP). In addition, unlike other characteristic ions of the organic sample, it is obvious that they mirror the desorption/ionization behavior of organic material that is either at the frontier with the metal islands or covers them (diffusion). Figure 4, parts a and b, shows the corresponding portions of the mass spectra of Au-metallized PP bombarded by Ga^+ and C_{60}^+, respectively. For gallium bombardment, the results obtained in a previous report (in which gold was thermally evaporated) are confirmed.[11] The mass spectrum observed under fullerene bombardment, however, is different. Instead of Au-cationized fragments directly mirroring the structure of the polymer, such as the repeat unit (C_3H_6) or its dimer (C_6H_{12}), one observes again that the dominant cationized fragments are strongly unsaturated ($AuC_2H_2^+$, $AuC_3H_2^+$). Even though the cationized repeat unit, $AuC_3H_6^+$, is present, its intensity is about 4 times lower than that of $AuC_3H_2^+$. This observation is probably connected to the effect described in Figure 3.

The partial mass spectra displayed in Figure 5 highlight other significant differences between gallium- and fullerene-induced desorption from Au-covered polyolefins. The bombardment of metallized PP and PE samples by gallium leads to the emission of a series of long-chain segments cationized by a metal ion, with the formula $AuC_{3n}H_{6n}^+$ for PP (Figure 5a) and $AuC_nH_{2n}^+$ for PE (not shown). These large chain segments, also observed upon thermal evaporation of Au, are very specific to the sample molecular structure.[11] In the mass spectrum obtained upon C_{60}^+ bombardment, these peaks are absent or have a very low intensity (Figure 5b). If there was a similar yield increase factor for those adducts peaks as the one measured for fingerprint peaks in the low-mass range of the spectrum, they should be off-scale in Figure 5b. Instead, the only intense peaks in that region correspond to

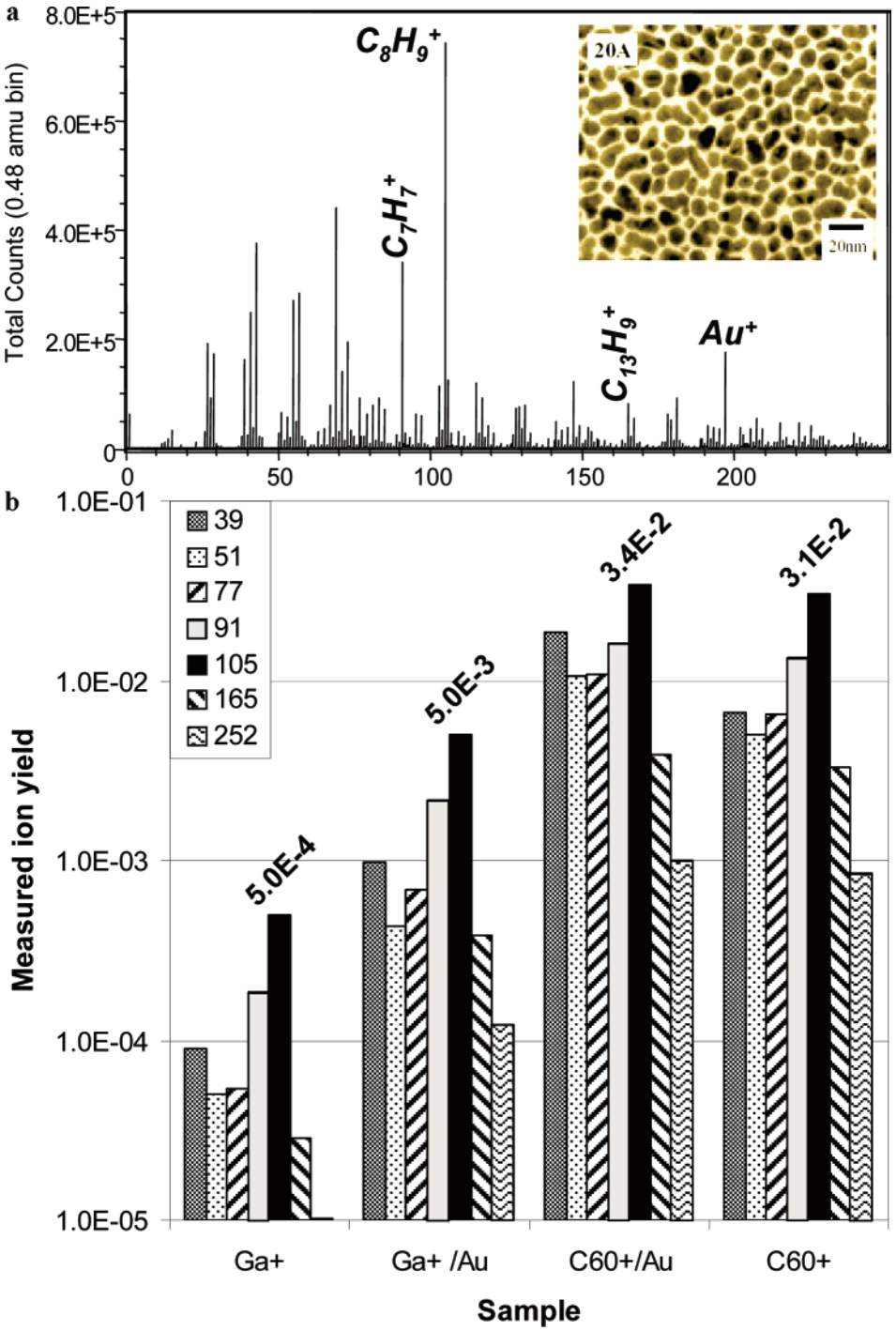

Figure 8. (a) Fingerprint positive secondary ion mass spectrum ($0 < m/z < 250$) of Au-metallized plasma polystyrene (PPS) sample upon 15 keV Ga^+ bombardment (1.5×10^8 PIs). Inset: TEM image of the sample microstructure. (b) Measured yields of PPS positive secondary ions obtained with different experimental conditions. The secondary ions are signified by their mass/charge ratio in the bar graphs ($C_3H_3^+$, $m/z = 39$; $C_4H_3^+$, $m/z = 51$; $C_6H_5^+$, $m/z = 77$; $C_7H_7^+$, $m/z = 91$; $C_8H_9^+$, $m/z = 105$; $C_{13}H_9^+$, $m/z = 165$; $C_{20}H_{12}^+$, $m/z = 252$).

gold cluster ions, adducts of the form $Au_xC_y^+$, and molecular ions of additives present in the polymer (Irgafos 168).[36] In general, we observe that all the Au-cationized species have comparatively lower intensities when fullerenes are used as projectiles.

To investigate the dynamics of the yield evolution upon metallization, PP films with 0, 5, 10, 20, and 40 Å of gold were prepared in the sputter-coater. These samples were metallized step by step, up to the maximum Au dose. The yield variation as a function of gold coverage is shown in Figure 6 for both Ga^+ and C_{60}^+ PIs. The difference is striking. With Ga^+, the fingerprint ion intensities increase steeply from 0 to 5−10 Å of gold, and then, the increase rate gradually levels off. With C_{60}^+, the measured yields decrease slightly but steadily from 0 to 40 Å of gold, confirming that gold metallization does not provide any enhancement and even tends to reduce the characteristic fragment ion yields. The ion yields of selected metal−organic adduct ions are presented in Figure 7 as a function of metal coverage for PP. Again, the evolution of these ion intensities is very dependent on

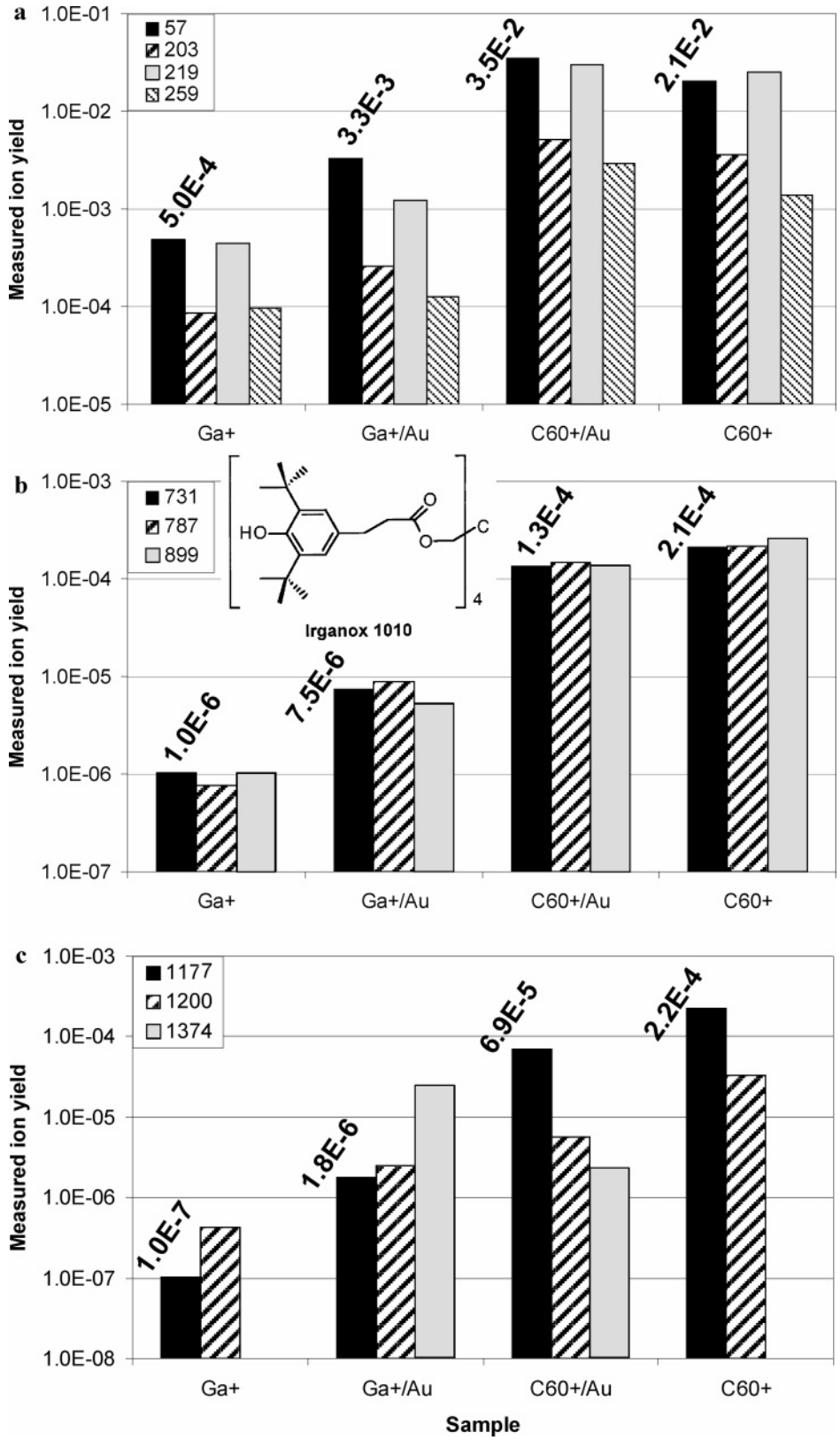

Figure 9. Measured yields of Irganox 1010 positive secondary ions obtained with different experimental conditions: (a) fingerprint ions; (b) large fragment ions; (c) parent-like ions. The secondary ions are signified by their mass/charge ratio in the bar graphs ($C_4H_9^+$, $m/z = 57$; $C_{14}H_{19}O^+$, $m/z = 203$; $C_{15}H_{23}O^+$, $m/z = 219$; $C_{17}H_{23}O_2^+$, $m/z = 259$; $(M - C_{17}H_{25}O_3 - 3C_4H_8)^+$, $m/z = 731$; $(M - C_{17}H_{25}O_3 - 2C_4H_8)^+$, $m/z = 787$; $(M - C_{17}H_{25}O_3)^+$, $m/z = 899$; M^+, $m/z = 1177$; $(M + Na)^+$, $m/z = 1200$; $(M + Au)^+$, $m/z = 1374$).

the type of projectile, as shown by the representative behavior of the Au-cationized repeat unit of PP, $AuC_3H_6^+$. Under Ga^+ bombardment, the yield of $AuC_3H_6^+$ increases almost linearly with the deposited gold quantity. This behavior also differs from that of pure fingerprint ions of PP such as those illustrated in Figure 6. In particular, the tendency of the yields to saturate, observed in

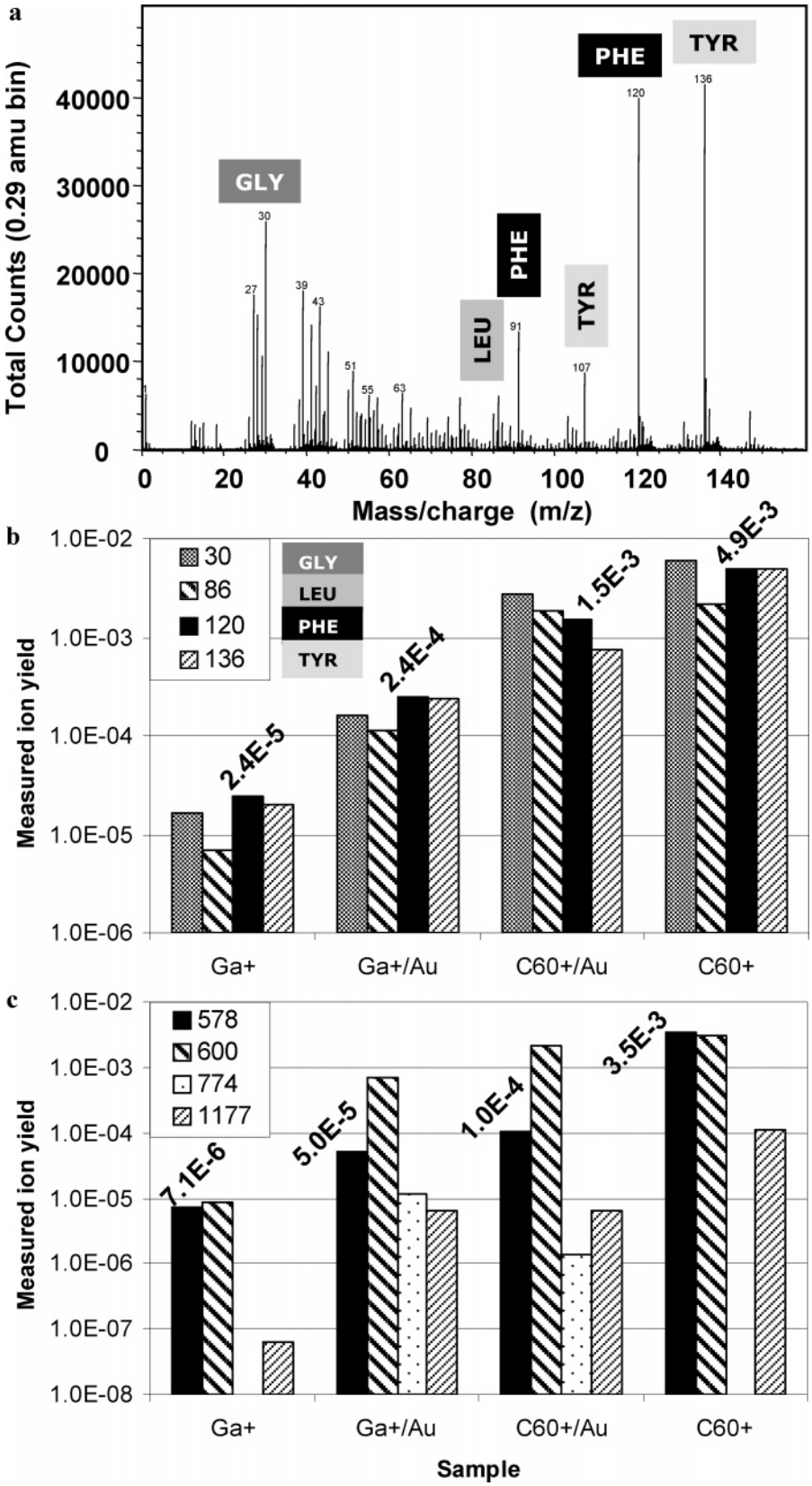

Figure 10. (a) Fingerprint positive secondary ion mass spectrum ($0 < m/z < 160$) of a leucine enkephalin overlayer adsorbed on Si upon 15 keV C_{60}^+ bombardment (3.1×10^6 PIs). (b and c) Yields of positive secondary ions sputtered from a dried droplet of leucine enkephalin acetate salt, measured under different experimental conditions. The secondary ions are signified by their mass/charge ratio in the bar graphs (CH_4N^+, $m/z = 30$; $C_5H_{12}N^+$, $m/z = 86$; $C_8H_{10}N^+$, $m/z = 120$; $C_8H_{10}NO^+$, $m/z = 136$; $(M + Na)^+$, $m/z = 578$; $(M - H + 2Na)^+$, $m/z = 600$; $(M + Au)^+$, $m/z = 774$; $(2M - 2H + 3Na)^+$, $m/z = 1177$).

Figure 6 for small hydrocarbons, does not exist for $AuC_3H_6^+$ and other metal−organic adducts of the same kind (not shown). In sharp contrast, for C_{60}^+ bombardment, the yield of $AuC_3H_6^+$ is almost constant over the entire range of gold coverage, from 5 to

40 Å. For the reasons mentioned earlier, the maximum observed for the 10 Å gold layer-equivalent might not be significant. Figure 7a also shows the evolution of the Au-cationized molecular ion of Irgafos 168, the antioxidant present in the PP sample, under Ga^+ bombardment. The signal corresponding to Irgafos 168 increases perfectly linearly with the deposited gold quantity. Figure 7b indicates that a similar linear increase occurs for the Au-cationized chain segments present in the mass spectrum of Ga^+-bombarded PP (Figure 5a). Interestingly, the yield of elemental gold ions tends to saturate, while that of PP and antioxidant-related ions continue to increase steadily. These typical behaviors will be discussed in the Mechanisms of Ion Emission section.

2. Plasma Polystyrene (PPS). Films of PS have been plasma-polymerized onto silicon wafers and 20 Å of gold (layer-equivalent thickness) were evaporated on their surface. The microstructure of the gold layer in a similar system (inset of Figure 8a), measured by TEM, was already presented in a previous study.[37] It consists of a network of coalescing islets with a characteristic size of about 10−20 nm. The positive mass spectrum of Au-metallized PPS obtained under Ga^+ bombardment, Figure 8a, is dominated by the peak at $m/z = 105$ ($C_8H_9^+$). As shown by the bar graph (Figure 8b), the peak pattern of the metallized sample closely mirrors that of a pristine sample, except that the measured yields are, on average, 1 order of magnitude larger, as was already observed for PE and PP. The use of C_{60}^+ as a PI source leads to a slightly different peak pattern, where the relative yields of $C_7H_7^+$ ($m/z = 91$) and $C_8H_9^+$ are lower in comparison with those of other ions such as $C_3H_3^+$ ($m/z = 39$), $C_4H_3^+$ ($m/z = 51$), and $C_6H_5^+$ ($m/z = 77$). This effect is more pronounced when the surface is covered by gold. Even though the yields of $C_7H_7^+$ and $C_8H_9^+$ are not significantly enhanced by gold, those of smaller characteristic ions are, as exemplified by the 3-fold yield increase measured for $C_3H_3^+$. This observation is reminiscent of the pattern change observed for PE and PP (Figure 2). It is remarkable that this effect does not occur under Ga^+ bombardment for any of the polyolefins.

Irganox Coatings. The progression of the fragment ion yields from an IRGA coating is shown as a function of sample treatment/projectile in Figure 9, parts a and b. At first sight, the "rule" observed for polyolefins also applies here: on average, 20 Å of gold provides a yield increase close to 1 order of magnitude for the metallized sample and the use of C_{60}^+ instead of Ga^+ leads to another leap of 1 order of magnitude. There are specific behaviors, though. For instance, when going from pristine to metallized Irganox under C_{60}^+ bombardment, the yields of characteristic fragments under $m/z = 300$, including the dominant $C_4H_9^+$ ($m/z = 57$) and $C_{15}H_{23}O^+$ ($m/z = 219$) (Figure 9a), increase by a factor between 1 and 2, while the yields of larger fragments in the range of $600 < m/z < 1000$ (Figure 9b) decrease by a factor in the same range. The local peak patterns, i.e., the relative intensities of the different ions in the considered regions, are only slightly affected. In addition to the molecular ion, which was of course absent in the mass spectrum of high-MW polyolefins, IRGA also allows us to consider the yield evolution of a couple of additional parent-like ions: $(M + Na)^+$ ($m/z = 1200$) and $(M + Au)^+$ ($m/z = 1374$) (Figure 9c). The three parent(like) ions are informative in that their yields display strongly different and specific variations. First, the positively charged molecular ion of Irganox, an odd-electron ion resulting from the loss of an electron by the molecule ($m/z = 1176.78$), is the one that is the most influenced by the change in the experimental conditions. The measured yield of this ion is multiplied by ~2200 from the pristine sample bombarded by Ga^+ to the pristine sample bombarded by C_{60}^+. The yield difference between the pristine and the Au-metallized sample upon C_{60}^+ bombardment is a factor of 3. Second, the yield of $(M + Na)^+$ increases by a much smaller factor than M^+, about 80, over the whole range of experimental conditions. Third, the case of the Au-cationized molecule shows an inversion in the order of the yields between Ga^+ and C_{60}^+, the intensity of $(M + Au)^+$ being 1 order of magnitude larger upon gallium bombardment. This observation strongly supports our conclusion drawn from the study of polyolefins, namely, that the intensity of metal-cationized organic molecules and fragments is not favored by the use of C_{60}^+ as a projectile.

Leucine Enkephalin Coatings. A dried droplet of an LE acetate salt was analyzed using the different sets of experimental conditions described in the Materials and Methods. Leucine enkephalin is a small peptide containing four different amino acids (Gly, Tyr, Phe, Leu). In the sequence, Gly appears two times. As a reminder, the microstructure of a similar sample metallized with a uniform layer-equivalent thickness of 20 Å Au was shown in Figure 1b. The most characteristic peaks of each of these amino acids have been reported in the literature,[38] and they are tagged in the reference fingerprint mass spectrum of Figure 10a, obtained upon C_{60}^+ bombardment of an ultrathin pristine sample adsorbed on Si. The evolution of these four characteristic fragment ions over the entire set of experimental conditions, for the thick LE salt sample, is shown in Figure 10b. The usual, drastic, yield increase is observed when going from Ga^+-bombarded pristine samples to Au-metallized samples (1 order of magnitude) and then to C_{60}^+-bombarded pristine samples (another order of magnitude). Between Ga^+ and C_{60}^+ bombardment, the low-mass fingerprint ions (Gly, Leu) tend to increase at the expense of the higher mass fragment peaks (Phe, Tyr). Therefore, one should be careful when it comes to the interpretation of such relative intensities while moving from a projectile to another. More important is the change of pattern occurring between the pristine and the Au-metallized sample upon C_{60}^+ bombardment. This change is not observed upon Ga^+ bombardment. The reason of this modification is unclear but suggests again that great care should be taken for the interpretation of such sample spectra: the variation only reflects a change of experimental condition and not a modification of the sample (structure, conformation). Conclusions concerning sample properties should only be drawn from spectra acquired with the same set of experimental conditions (projectile, sample preparation).

The major parent-like ions sputtered from an LE salt sample are observed at $m/z = 578$ [$(M + Na)^+$] and $m/z = 600$ [$(M - H + 2Na)^+$], instead of the protonated molecule expected at $m/z = 556$ (present but weak). The behavior of these two ions, however, is different (Figure 10c). Under Ga^+ bombardment, both

(36) Médard, N.; Poleunis, C.; Vanden Eynde, X.; Bertrand, P. *Surf. Interface Anal.* **2002**, *34*, 565.

(37) Felten, A.; Gamby, S.; Bittencourt, C.; Brison, J.; Houssiau, L.; Pireaux, J.-J. Presented at the Sixth International Symposium on Ionizing Radiation and Polymers, Houffalize, Belgium, September 2004.

(38) Vickerman, J. C., Briggs, D., Henderson, A., Eds. *The Static SIMS Library*; SurfaceSpectra Ltd.: Manchester, U.K., 1999.

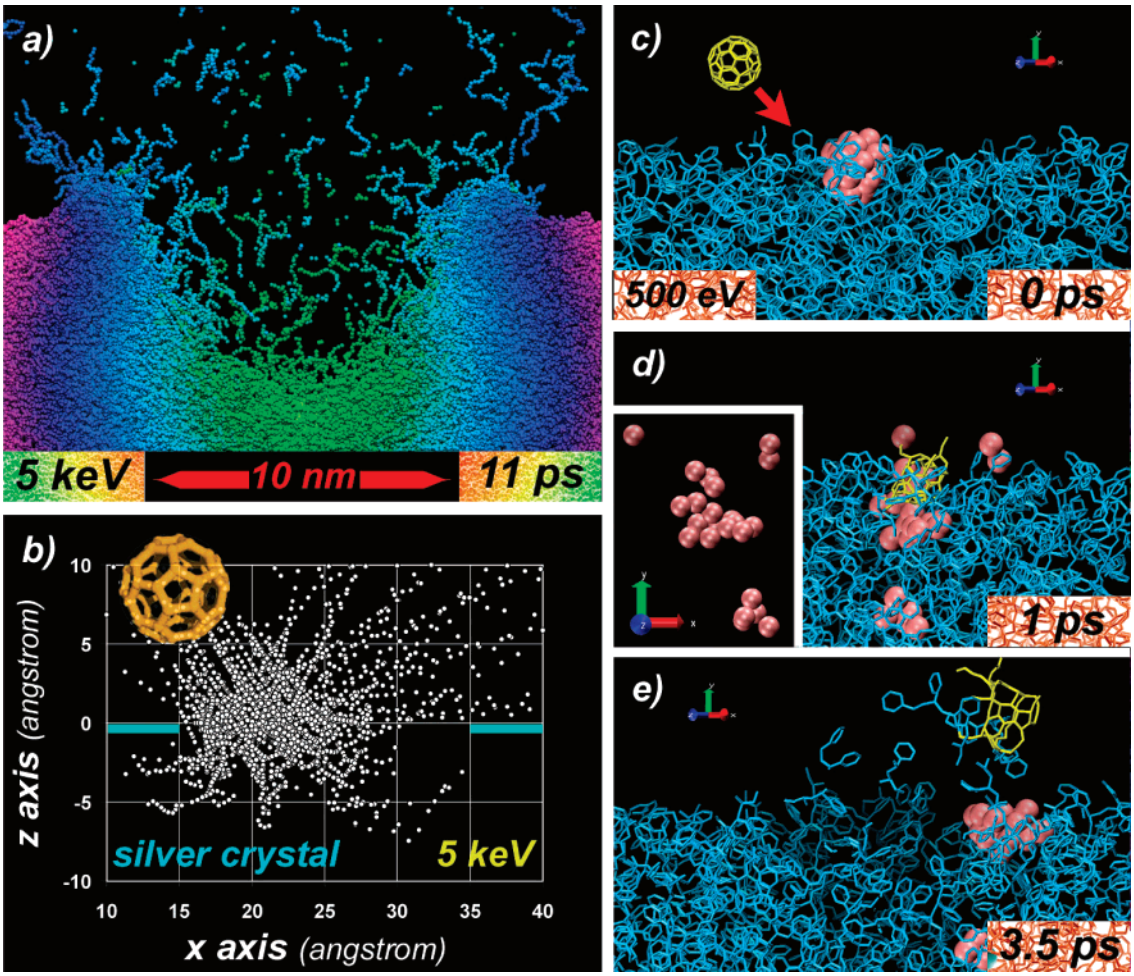

Figure 11. Molecular dynamics simulations. (a) Side view (11 ps after impact) of the crater formed in an amorphous icosane ($C_{20}H_{42}$) sample surface by a 5 keV C_{60} projectile (normal incidence). The sample atoms are color coded from green to purple as a function of the distance from the center of the sample at 0 ps. (b) Trajectories of the C atom constituents of a 5 keV C_{60} projectile impinging on a silver surface with a 45° incidence angle (from 0 to 200 fs after impact). (c−e) Snapshots of the molecular dynamics for a 500 eV C_{60} projectile (45° incidence) impinging on a Ag_{23} cluster embedded in an amorphous organic substrate made of polystyrene tetramers. The C−C bonds of the projectile and the sample are yellow and blue, respectively. The silver atoms are pink spheres. The hydrogen atoms are omitted for clarity. The inset of panel d shows a different view of the smashed silver cluster at 1 ps (see refs 3, 31, 40, and 42 for more details).

of their yields increase after metallization, by markedly different factors (~7 vs ~80). Under C_{60}^+ bombardment, the intensity of $(M + Na)^+$ decreases largely, while the intensity of $(M - H + 2Na)^+$ is only slightly reduced. The largest yield enhancement concerns the dimer-like ion $(2M - 2H + 3Na)^+$ at $m/z = 1177$. With respect to Ga^+ bombardment, gold metallization leads to an increase of 2 orders of magnitude, while fullerene projectiles induce a yield increase of more than 3 orders of magnitude. For all these ions, metallization does not constitute an interesting route when fullerenes are used as PIs. Moreover, as observed with the other investigated samples, gold adduct ions such as $(M + Na + Au)^+$ ($m/z = 774$) are not favored by C_{60}^+ bombardment. From a fundamental viewpoint, all these evolutions indicate that different channels of desorption/ionization are favored with different projectiles (Ga^+ vs C_{60}^+). In the discussion of Mechanisms of Ion Emission section, we argue that some of the observed ionization effects might directly arise from the different dynamics of projectile−solid interaction unfolding with atomic and cluster projectiles.

Mechanisms of Ion Emission. Several questions have been raised along the presentation of the results that deserve to be addressed if one wants to gain a better understanding of the effects of the projectile in MetA-SIMS. The most obvious one concerns the explanation of the—almost general—absence of yield enhancement generated by the condensation of the metallic overlayer when C_{60}^+ is used as a PI (i). In addition, while organic ions show a large yield enhancement when going from Ga^+ to C_{60}^+ projectiles, whether the surfaces are metallized or not, the yields of Au-cationized ions are often lower with C_{60}^+ than Ga^+ projectiles (ii). The very different evolution of the yields as a function of the deposited gold quantity also deserves an explanation (iii). Secondary issues relate to (iv) the very different yield evolutions observed for different parent-like ions when they can be measured and (v) the degree of fragmentation under different experimental conditions, mirrored by the yields of small versus large ions and of unsaturated versus saturated ions in the mass spectra.

Tentative interpretations for the MetA-SIMS effect, in particular the proposed diffusion of organic molecules on the clusters,[17,24] involve the close proximity of the metallic and the organic phase at the microscopic level. These explanations should be supported by observations of the metallized sample microstructure. According to the SEM (Figure 1b) and TEM (Figure 8, inset) images of

the metallized organic samples, the sputter-coated/thermally evaporated gold overlayers are made of a collection of nanoparticles of ~20 nm characteristic length, sometimes coalesced into larger islands. In comparison with other quantities of deposited metal,[39] this configuration ensures many connection areas between the metallic islets and the bare organic sample matrix. The other property of this specific microstructure, in contrast with lower quantities of gold that lead to a distribution of sparse gold islets in an organic "sea", is that it favors the percolation and evacuation of electric charges,[24] an invaluable advantage for the analysis of bulk insulators such as the PP and PE samples chosen for this study.

Coming to the mechanistic explanation of molecular ion emission and question (i), let us first consider the desorption stage of the process. The increased desorption yield observed with fullerenes instead of monatomic projectiles has been explained by mechanistic arguments. As shown by recent molecular dynamics simulations, energetic monatomic ions are able to penetrate deep into hydrocarbon samples such as PS, where most of there energy is "wasted" via the creation of bond scissions and damage in the depth of the sample.[31,40] Only a fraction of their energy is backscattered and induces molecule and fragment ejection. In contrast, it has been shown that isoenergetic fullerenes deposit their energy in the topmost layers of the samples, leading therefore to large emission yields.[3,40,41] Organic molecules are transferred into the gas phase from a superheated liquid-like region formed around the impact point, and as a result, a large crater forms in the surface of the sample. For the bombardment of an icosane molecular solid by 5 keV fullerene ions, the diameter of the crater is about 10 nm (Figure 11a). Simulations have also shown that, under monatomic ion bombardment, heavy metal targets were beneficial to induce the emission of large molecules, via the collective upward motion of substrate atoms.[42] Indeed, in a fraction of the trajectories, the energy of the projectile and the recoil atoms is very efficiently trapped in the surface region and subsequently backscattered. In contrast, it is now clear, however, that metallic substrates are not beneficial for the desorption of molecular overlayers upon C_{60} bombardment.[43] In fact, for benzene and PS adsorbed on silver, the yield enhancement ratio is very low—even smaller than unity—when going from 15 keV Ga^+ to 15 keV C_{60}^+ bombardment (203% for benzene and 81% for PS).[44]

As an example, 5 keV fullerene projectiles impinging on a silver crystal create a 2.5 nm diameter crater,[45] displacing thereby a volume of material that is about 60−70 times smaller, and a mass that is roughly 6−7 times smaller, than the case of icosane molecular substrates.[3] Part of the explanation of this difference is the mass mismatch of carbon and metal atoms that leads to an efficient reflection of the projectile atoms (and a significant fraction of their energy) in the case of the metallic substrate. This situation is exemplified in Figure 11b, where the successive positions of the C atom constituents (atom tracks) of a 5 keV fullerene are shown over a 200 fs time range. The fullerene explodes upon impact with the silver surface, and many of its C atoms are directly backscattered in the vacuum. The observed behaviors are of course dependent on the projectile energy, and one could argue that C_{60} might become comparatively more efficient at sputtering metal samples with increasing energy, when the projectile constituents implant more in the substrate. Another obvious factor limiting the yield for metallic surfaces is their much higher cohesive energy. In comparison, fullerenes can easily displace and shatter small metal clusters *weakly* attached to an organic substrate, a situation that leads to very high yields of metal clusters in SIMS.[46] Figure 11c−e shows the time evolution of a MD trajectory in which a relatively low-energy (500 eV) C_{60} projectile impinges on a Ag_{23} cluster embedded in the surface of a PS tetramer molecular solid. The silver cluster breaks up under the collective action of the C constituents of the projectile. After 1 ps, a silver atom and a dimer are emitted, while two larger daughter clusters continue sliding/rolling in the soft PS surface, much like rocks thrown in the sand or the snow. The slowing of the larger cluster even induces the emission of an intact PS tetramer and smaller fragments. It is interesting to note (Figure 11e) that, in this energy regime, the constituents of the C_{60} projectile remain bound after reflection from the surface. In contrast with such small clusters embedded in an organic surface, when a thin molecular overlayer is adsorbed on a metallic substrate (or a larger metal islet), most of the dynamics is ruled by the metal, the disturbed volume is comparatively small, and the number of ejected molecules is limited.[44]

One may then wonder if these conclusions still apply after the charge formation/transfer processes required prior to any SIMS observation. SIMS experiments indicate that certain trends derived from the simulations for neutral particles extend indeed to ions. The mass spectra of PS oligomers adsorbed on Ag as a thin layer from a very dilute solution or, as a thicker coating from a more concentrated solution, are shown in Figure 12. The characteristic fragments of PS, especially $C_7H_7^+$, are intense in both cases. The mass spectrum of the thick coating displays large molecular ion peaks mirroring the mass distribution of the oligomers (Figure 12c), while the one of the thin layer shows mostly silver-cationized molecules, with masses shifted by 107/109 Da with respect to the mass of the oligomers. Figure 12 confirms that, under fullerene bombardment, the influence of the silver substrate does not lead to any yield enhancement for the fingerprint fragment ions and for the molecular ion ($m/z = 474$). In contrast, it has been shown in several occurrences and for various organic molecules,[47−49] that, upon monatomic ion bombardment, the yield of molecular and fragment ions could be up to 2 orders of magnitude larger in the overlayer on metal than in the bulk organic substrate situation. This large yield increase cannot be solely explained by the desorption argument quoted before but requires a contribution of ionization. A reasonable physical reason, based on electronic

(39) Zaporojtchenko, V.; Zekonyte, J.; Wille, S.; Schuermann, U.; Faupel, F. *Nucl. Instrum. Methods Phys. Res., Sect. B* **2005**, *236*, 95.
(40) Delcorte, A. *Phys. Chem. Chem. Phys.* **2005**, *7*, 3395.
(41) Smiley, E.; Postawa, Z.; Wojciechowski, I. A.; Winograd, N.; Garrison, B. J. *Appl. Surf. Sci.* **2006**, *252*, 6436.
(42) Delcorte, A.; Garrison, B. J. *J. Phys. Chem. B* **2000**, *104*, 6785.
(43) Czerwinski, B.; Delcorte, A.; Garrison, B. J.; Samson, R.; Winograd, N.; Postawa, Z. *Appl. Surf. Sci.* **2006**, *252*, 6419.
(44) Czerwinski, B.; Samson, R.; Garrison, B. J.; Winograd, N.; Postawa, Z. *Vacuum* **2006**, *81*, 167.
(45) Postawa, Z.; Czerwinski, B.; Szewczyk, M.; Smiley, E. J.; Winograd, N.; Garrison, B. J. *J. Phys. Chem. B* **2004**, *108*, 7831.
(46) Delcorte, A.; Poleunis, C.; Bertrand, P. *Appl. Surf. Sci.* **2006**, *252*, 6494.
(47) Hagenhoff, B. Noble Metal Supports in Organic SIMS. In *The Static SIMS Library*; Vickerman, J. C., Briggs, D., Henderson, A., Eds.; SurfaceSpectra: Manchester, U.K., 1999; p 39.
(48) Delcorte, A.; Segda, B. G.; Bertrand, P. *Surf. Sci.* **1996**, *381*, 18.
(49) Delcorte, A.; Bertrand, P. *Surf. Sci.* **1998**, *412/413*, 97.

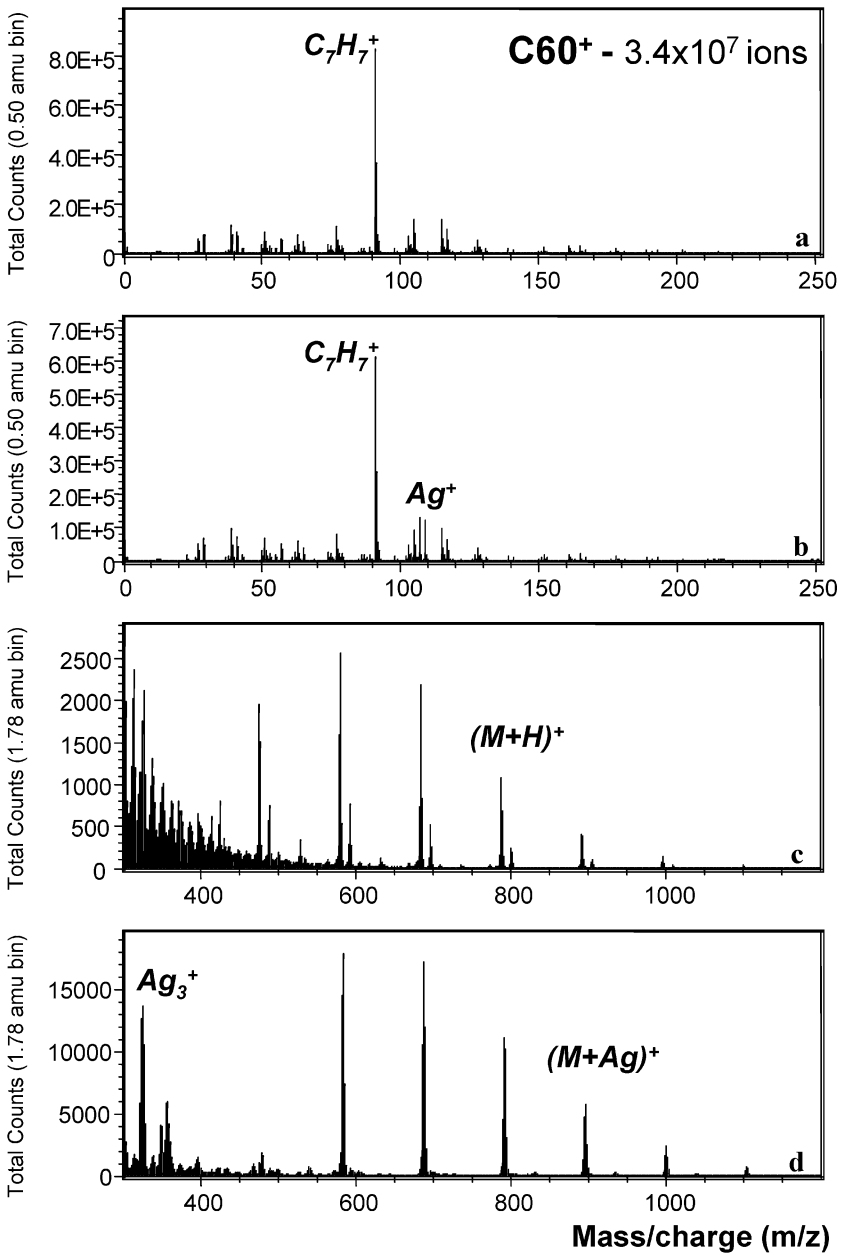

Figure 12. C_{60}^+-induced positive secondary ion mass spectra of (a and c) a thick (>10 nm) PS (M_n = 550 Da) coating on silver and (b and d) a thin (monolayer range) PS (M_n = 550 Da) coating on silver.

structure argument, is that the ionization potential of the organic molecules is lowered by the proximity of the metal (splitting of the HOMO−LUMO levels within tunneling range of the metal).[50] This mechanism has been verified for the case of the MALDI matrix molecule, 2,5-dihydroxybenzoic acid (DHB), in contact with metallic steel and gold.[51] Under C_{60}^+ bombardment, the specific ionization effects related to the metal substrate are probably "masked" by the very high yields already observed for the pristine organic sample.

All the above explanations nicely accommodate the MetA-SIMS observations and seem to adequately answer question (i), under the assumption that the organic molecules diffuse on the metal islets. Our results concerning the dynamics of the yield increase as a function of gold coverage for PP support the hypothesis of diffusion of organic material over the gold layer (iii). In particular, the steady increase of the Au-cationized Irgafos 168 and PP chain segments up to very large gold doses is reminiscent of the phenomenon observed with short PS oligomers in a previous paper and would be hard to explain otherwise.[11] In the present case, diffusion should be enhanced by the regime of metallization that allowed the system to relax after each step of sputter-coating (see the Materials and Methods). Upon repeated metallization steps, the system would gradually evolve from the thick organic layer regime to the overlayer-on-metal regime, beneficial upon Ga^+ bombardment and detrimental upon C_{60}^+ bombardment (question iii). Even though the diffusion effect is clearly supported in the case of PP, it seems important to mention that most of the conclusions of the previous paragraphs should also apply for

(50) Knochenmuss, R. *Anal. Chem.* **2004**, *76*, 3179.
(51) McCombie, G.; Knochenmuss, R. *J. Am. Soc. Mass Spectrom.* **2006**, *17*, 737.

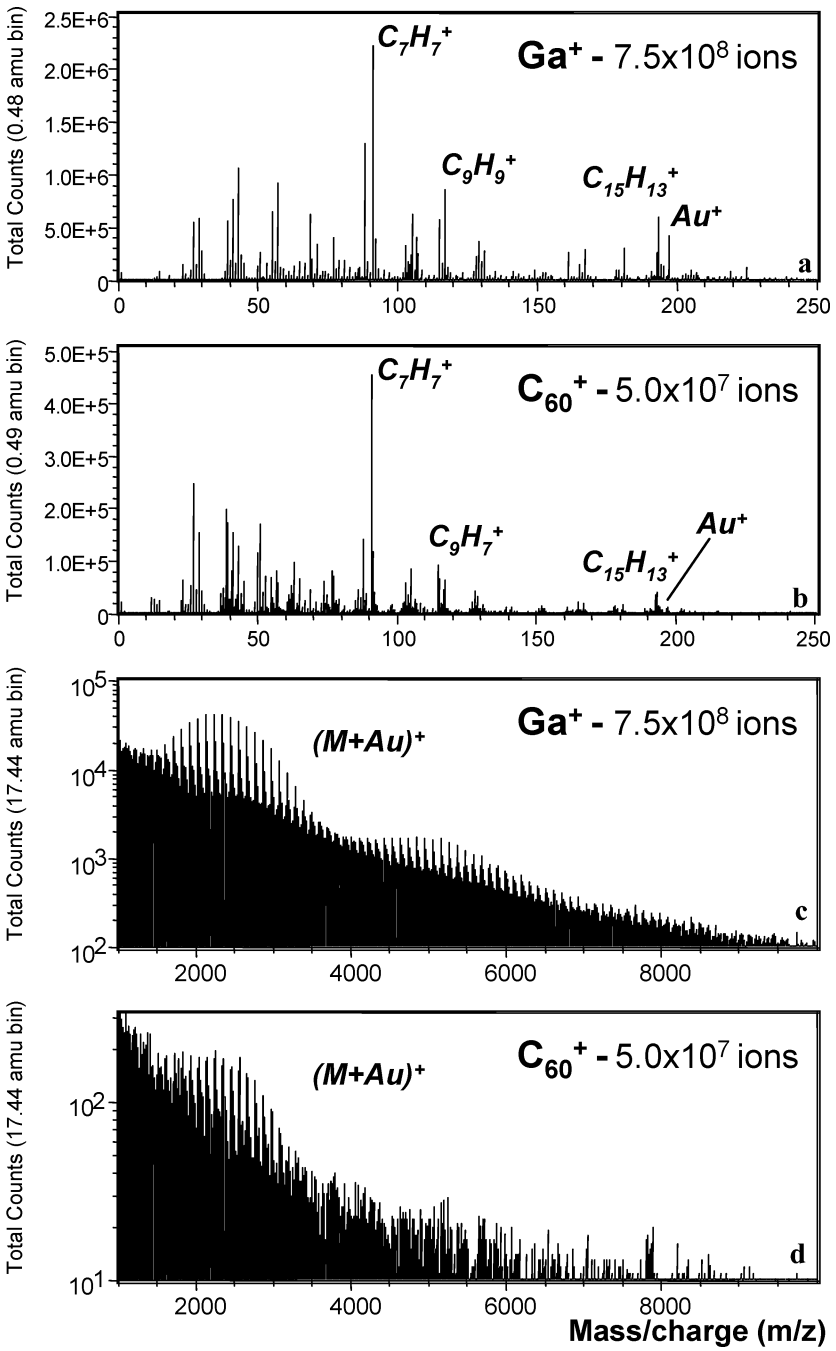

Figure 13. Positive secondary ion mass spectra of thin coatings (monolayer range) of a mix of PS standards (M_n = 2180, 4760, 8000, and 12 400 Da) adsorbed on gold: (a and c) 15 keV Ga^+ and (b and d) 15 keV C_{60}^+ bombardment.

organic molecules *neighboring* metal nanoparticles (both the desorption and the ionization effects).

The relatively low efficiency of fullerene ions to induce metal cationization (ii) can be checked by looking at thin overlayers on metal surfaces. Figure 13 shows the mass spectra of a mix of PS standards adsorbed on a metal-evaporated gold substrate. The limited ~3-fold increase of the fragment ion yields when going from Ga^+ to C_{60}^+ projectile (Figure 13, parts a and b), as opposed to the 2 orders of magnitude enhancement measured for thick samples, confirms our previous observations. In comparison, the high-mass range of the spectra (Figure 13, parts c and d) shows that the yield of Au-cationized PS oligomers is *reduced* by about 1 order of magnitude using C_{60} instead of gallium. The observed reduction is in agreement with the MetA-SIMS results (Figures 5, 7, 9, and 10). Its explanation is not clear at this stage, but as a complement of information, it should be noticed that the yield enhancement of monatomic Au^+ is also very limited. Among the possible interpretations, the lower ionization probability of the metal or the lack of spatial/temporal correlation between single metal atoms and intact molecules during the ejection process might play an important role.

The different dependence of parent-like ion yields on the experimental conditions (iv) is difficult to rationalize, especially because they also appear to be sample-dependent (evolution of the $(M + Na)^+$ ion). Nevertheless, the recent literature provides us with information that could also be relevant for the elucidation

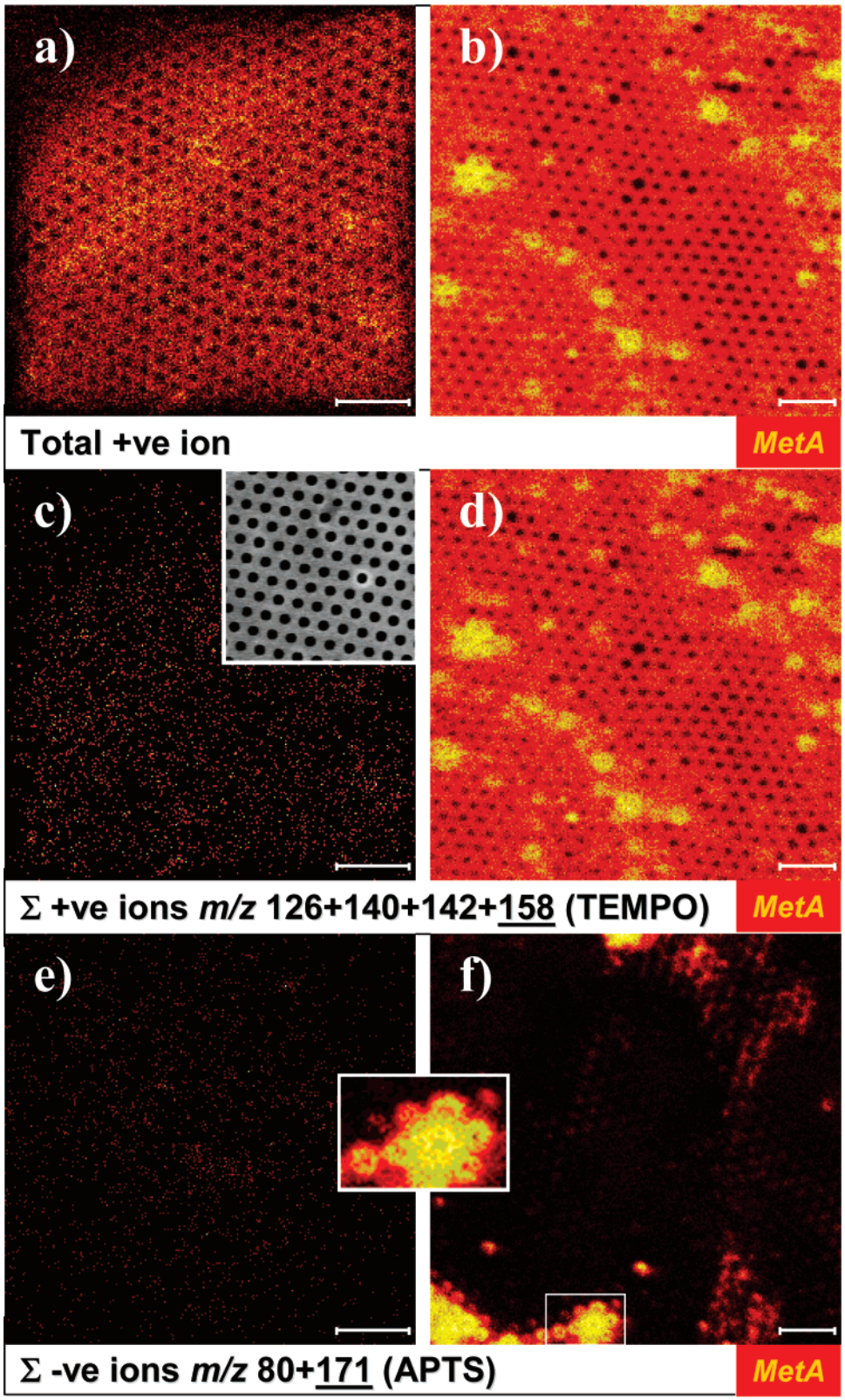

Figure 14. TOF-SIMS images (scale bars are 10 μm long) of a microstructured sample of functionalized polystyrene (see text for details) obtained upon 25 keV In^+ bombardment: (a, c, e) pristine sample; (b, d, f, and inset of e, f) Au-metallized sample. The inset of (c) shows the SEM image of a similar sample. The ion peaks used to obtain the images are signified by their mass/charge ratio under each set of pictures (see Table 1). The underlined numbers refer to the mass/charge of the entire TEMPO residue (158) and APTS molecule (171). The primary ion doses applied for the acquisition of the images are listed in Table 1. Ion fluences: (a−d, f) 2.1×10^{13} ions/cm^2; (e) 3.3×10^{13} ions/cm^2.

of these effects. For instance, it has been shown that 20 keV C_{60} projectiles create a much larger number of protons in the surface of ice samples than atomic projectiles.[52,53] In the case of PS molecular samples, recent MD simulations also show that tens of C−H bonds are broken by 10 keV C_{60} projectiles around their impact point.[40] The energized volume may therefore appear as a

dense localized plasma where ions, radicals, and molecules coexist. In addition, the large sputtering yields induced by fullerenes and the MD simulation movies[3] indicate the development of a plume above the projectile impact point, a situation that should favor interactions/reactions between sputtered species, in contrast with the case of atomic projectile bombardment. These pronounced differences in the *dynamics* of sputtering may well be at the origin of the relative differences observed in the proportions of measured ions.

Most of the results obtained for polyolefin substrates (Figures 2−4, 8) indicate that the levels of fragmentation and dehydrogenation of the sputtered ions are larger with C_{60}^+ than Ga^+ and that they are further modified by the presence of gold (our question v). It has been recently shown that, for each impact into an organic substrate, keV fullerenes generate a large number of C−C and C−H bond scissions[40] and fragment species[41] in a spherical region surrounding the track of the projectile, in the topmost layer of the sample. Most of these damaged species are sputtered right away, within the same bombardment event, which contributes to explaining the ability of C_{60} to depth-profile organic samples with partial persistence of the molecular information. Concerning the static SIMS regime, however, it is not surprising that this large production/emission of fragments is directly translated in the mass spectrum through intense fragmentation peaks. The different mechanisms of ion−solid interaction using Ga^+ versus C_{60}^+ PIs simply lead to a different balance of saturated versus unsaturated and large versus small fragments. The practical implication, however, is that static SIMS using C_{60}^+ projectiles for high-MW polyolefins leads to mass spectra that mirror somewhat less the molecular structure of the sample. Therefore, fullerenes do not seem to be the best projectiles for this application.

Practical Implications: Which Projectile for MetA-SIMS? Most of our results show that it is not beneficial to use a C_{60}^+ primary beam for MetA-SIMS (at least with an energy around ∼15 keV), because the highest yields are already attained on pristine samples using fullerene projectiles. In the rare cases where one observes a metal-related yield enhancement upon C_{60}^+ bombardment, it is very limited and does not justify such a preparation procedure and the risks of sample contamination/damage that it might induce. On the other hand, the results obtained on PP (Figure 2) indicate that the yield enhancement observed with gallium exists also for heavier monatomic projectiles like In^+. This observation points to the additivity of the projectile and the gold layer benefits in that case. Therefore, heavier projectiles should be preferred to lighter ones for imaging with MetA-SIMS, provided that the beam focusing is comparable. In Figure 14, we exemplify the combination of MetA-SIMS with 25 keV In^+ projectiles for surface imaging. Highly ordered microstructured films were prepared by casting from a volatile solvent in the presence of humidity, a procedure called breath figure imprinting. For the sample imaged in Figure 14, a honeycomb structure was obtained by activation of TEMPO-terminated PS with PTSA. The total positive ion image is displayed in Figure 14, parts a and b, with and without metallization. The cumulated yield of ions in the range of $0 < m/z < 400$ increases from 4.3×10^{-4} to 1.3×10^{-2} after gold deposition. The yield enhancement of the fingerprint ions of PS is relatively limited (<10), as exemplified by the case of $C_7H_7^+$ (Table 1). In contrast, the yield enhancement of the most characteristic peaks corresponding to the TEMPO chain ends and to the PTSA molecules is dramatic, as shown in Figure 14c−f and Table 1. The largest enhancement is measured for the fragment ion of TEMPO, $C_9H_{20}N^+$, and reaches almost 3 orders of magnitude. These very different enhancement factors observed for the PS and TEMPO fragments suggest a strong dependence of the ionization probability increase on the type (and on the ionization mechanism) of the sputtered species when going from pristine to Au-metallized samples. Figure 14 and Table 1 also show that MetA-SIMS can induce large yield enhancements for negatively charged secondary ions, an observation already reported for polymer antioxidants in a previous article[11] but that does not seem to be valid for all types of molecules.[17]

Table 1. Statistics of Characteristic Ion Yields and Yield Enhancement Factors for the Pristine and Au-Metallized Microstructured PS Samples (See Figure 14)

m/z	formula	yield (pristine) ($\times 10^{-6}$) [1][a]	yield (MetA) ($\times 10^{-6}$) [2][a]	enhancement factor [2]/[1]
positive ions		(7.6×10^8 PIs)	(1.2×10^9 PIs)	
0−400		427	12500	29
91	$C_7H_7^+$	32	139	4.4
126	$C_8H_{16}N^+$	1.7	230	135
142	$C_9H_{20}N^+$	1.7	1700	980
158	$C_8H_{16}NO^+$	0.7	310	428
negative ions		(1.2×10^9 PIs)	(1.2×10^9 PIs)	
0−400		5490	12200	2.2
80	SO_3^-	0.7	303	421
171	$C_7H_7SO_3^-$	1.5	309	204

[a] The yield is calculated as the measured number of secondary ions per primary ion (PI), without any correction for the instrument transmission and detection probabilities.

In line with the above discussion, cluster ions made of heavy elements might also constitute more appropriate projectiles for MetA-SIMS than fullerene clusters, at least in the usual energy range of SIMS measurements (<50 keV). One recent report by McDonnell et al. shows that, for a tissue section under Bi_3^{2+} projectile bombardment, the characteristic, high-mass cholesterol and lipid ions undergo a yield enhancement of a factor of 2−5 (depending on the considered ion) when going from the pristine to the Au-metallized material.[23] This observation, contrasting with our results with fullerene PIs, supports the idea that mass ratio between the projectile and the target elements plays a significant role. Therefore, it is to be expected that higher atomic mass Bi_n^+ and Au_n^+ might provide better results under MetA-SIMS conditions. Another difference that might be influential relates to the energy of the beam (25 keV for our imaging with the In^+ beam and 40 keV for the Bi_3^{2+} beam in ref 23). High-energy clusters, including fullerenes, should be able to shatter a 10−20 nm nanoparticle such as those observed in Figure 1. Indeed, MD simulations[45,54] show that 15−16 keV C_{60} and Au_4 clusters create craters in metals that displace respectively 1590 Ag (5.4 nm diameter crater) and 620 Au atoms. In the case of the C_{60} bombardment on Ag, the number of displaced atoms seems to

(52) Wucher, A.; Sun, S.; Szakal, C.; Winograd, N. *Anal. Chem.* **2004**, *76*, 7234.
(53) Winograd, N.; Postawa, Z.; Cheng, J.; Szakal, C.; Kozole, J.; Garrison, B. J. *Appl. Surf. Sci.* **2006**, *252*, 6836.
(54) Colla, Th. J.; Aderjan, R.; Kissel, R.; Urbassek, H. M. *Phys. Rev. B* **2000**, *62*, 8487.

evolve almost linearly with the projectile energy (~100 displaced crater atoms per keV).[45] The difference between the gold and silver target results also points to an influence of the target elemental mass. Therefore, alternative to an increase of the projectile energy, the use of a lighter metal such as Ag for metallization might have interesting consequences under C_{60} bombardment. The effects of these three parameters, cluster projectile nature, projectile energy, and deposited metal atomic mass, should be carefully tested in order to obtain a more complete view, and a better understanding, of the phenomena at play and the corresponding gain for analysis that should be expected.

CONCLUSION

Upon 15 keV buckminsterfullerene bombardment of most organic samples (polymers, molecular solids, peptide coatings), gold metallization of the surface (MetA-SIMS) does not provide a significant enhancement of the characteristic fragment and parent-like ion yields. Even though many of the observed effects are sample-specific, the trend exemplified with PP bulk samples is that, while gradual coverage of the surface by gold leads to increasing organic ion yields using Ga^+ projectiles, it degrades the secondary ion yields upon C_{60}^+ bombardment. The explanation of this effect was based on arguments involving recent MD simulation and experimental results. More precisely, the probable diffusion of molecules on the metal islets (not *absolutely* required) and, especially, the relatively limited efficiency of C_{60} projectile at sputtering high yields of intact organic molecules in such a case figure have been invoked. However, the research route involving the combination of cluster projectiles and MetA-SIMS is not closed yet, as suggested by a recent report using Bi_3^{2+} ions.[23] As explained in the discussion, an exhaustive view of the effects and their mechanisms will require the systematic investigation of various parameters such as the cluster projectile type, the projectile energy, and the type of metallic overlayer used in the experiments. Also on the agenda, proper attention should be devoted to the less studied effect of MetA-SIMS on the yield of negatively charged fragment and parent-like ions. Such investigations pave the way to the optimization of the MetA-SIMS procedure.

ACKNOWLEDGMENT

A.D. acknowledges the Belgian Fonds National pour la Recherche Scientifique for financial support. The Région Wallonne of Belgium is acknowledged for supporting S.Y. The TOF-SIMS equipment was acquired with the support of the Région Wallonne and FRFC-Loterie Nationale of Belgium. The C_{60}^+ source was obtained with the support of the FRFC. The European Community is acknowledged for funding N.N., N.W., and part of this work through the Network of Excellence NANOBEAMS.

Received for review December 20, 2006. Accepted February 27, 2007.

AC062406L